Low Speed Bicycle Stability: Effects of Geometric Parameters

Jason Moore
MAE 223
August 2006

Introduction

It would be helpful for bicycle designers, especially novices, to have a set of scientifically backed guidelines that could direct them in choosing appropriate geometrical parameters to obtain desired handling characteristics. Several critical geometrical parameters of standard bicycles have been identified over time and their significance has normally been explained through experience and pseudoscientific methods. Although many dynamic studies have been done in the realm of two-wheeled single-track vehicles, easily interpreted, consistent, and somewhat complete layman's guidelines haven't seemed to emerge from these studies.

The following analysis will attempt to extract some guidelines for choosing four important parameters in bicycle design. A three-degree of freedom idealized bicycle model will be developed and analyzed. Two important eigenmodes will be determined from the linearized version of the model. From these eigenmodes two critical velocities for stability will be determined for various geometric parameter changes. An interpretation of these critical velocities will lead to a limited understanding of the handling qualities of various bicycle designs.

Bicycle Parameters

For this study a standard road bicycle will be used as a base bicycle model. Figure 1 shows the basic shape of a diamond frame road bike with various important dimensions labeled.
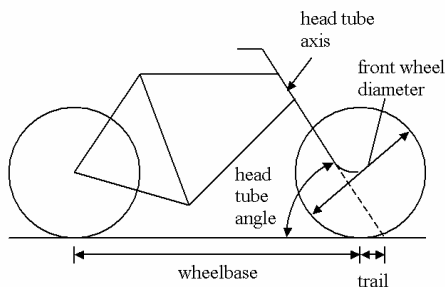

Figure 1: Basic bicycle dimensions

The four parameters that are of particular interest are the front wheel size, the wheelbase, the head tube angle, and the trail. Each of these parameters will be varied through a realistic range for the base bicycle model and the critical velocities extracted for each variation. To do this a variable geometric model of the bicycle and rider was developed that calculated all of the required parameters for the dynamic model described in the following section.

A bicycle and rider geometric model was constructed from a set of grid points and simple geometric shapes. Figure 2 depicts the model. The bicycle frame is made of tubes, the wheels are tori, and the rider is a combination of rectangular prisms, cylinders, and a sphere. The four rigid bodies that make up the dynamic model are shown each with different colors.
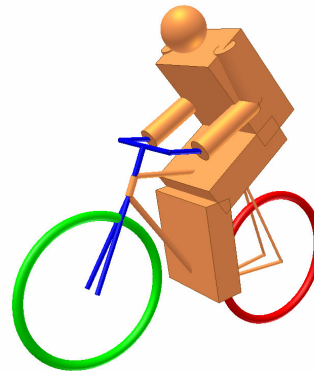

Figure 2: Simple bicycle geometric model

A MATLAB program was developed that took the basic dimensions typically provided by a bicycle manufacturer along with the rider's dimensions and generated all necessary geometric, mass, and inertial properties needed for the dynamic model. The program is provided in Appendix 1, bike_inertia.m. It converts the common dimensions to a three dimensional grid and lays out the appropriate 3D solid (torus, tube, prism, etc.) along the points. Once this is done, the centers of mass of each element are calculated, along with the centers of mass for each rigid body. Then the local inertial properties of each element are calculated which

1

are then transformed and translated to the appropriate reference frame for each rigid body using direction cosines and the parallel axis theorem. Finally the parameters used in the AUTOLEV code described in the following section are computed.

Model Description

Many different models have been developed for bicycles and motorcycles. They range from simple one-degree of freedom models to multiple degree of freedom models with various elastic, and damping effects, and tire characteristics. The model chosen for this study is a three-degree of freedom model made up of four rigid bodies: the front and rear wheels, the front fork, and the rear frame/rider. The bodies are connected to each other by three revolute joints; one about the head tube axis and two about the wheel axes.

Many assumptions have been made to keep the model simple and they are as follows:

- The cycle is traversing a flat plane
- The wheels are knife edge discs that roll without slip
- The rider is rigidly fixed to the rear frame and is riding no-handed
- No viscous damping or elastic members are included, this system is perfectly rigid
- The three revolute joints are frictionless

The model was developed using Kane's methods with the assistance of the program AUTOLEV. The following descriptions use the syntax commonly associated with Kane's methods.
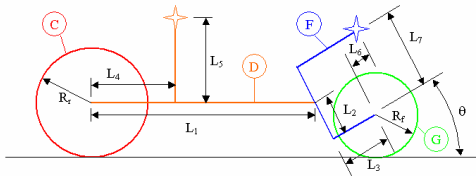

Figure 3: AUTOLEV representative model with constants labeled

Each rigid body was given an alphabetical name. The rear wheel is C, the frame/rider is D, the front fork is F, and the front wheel is G. These are depicted in Figure 3 along with ten constants that describe the bicycle geometry. It is assumed that the bicycle is in its nominal upright position in the following descriptions of the constants.

- R_r: rear wheel radius

- R_f: front wheel radius
- θ: complement of the head tube angle
- L_1: the horizontal distance from the center of the rear wheel to the intersection of the head tube axis
- L_2: the distance along the head tube axis from the previous intersection point to the intersection of the L_3 line
- L_3: the perpendicular distance from the center of the front wheel to the head tube axis (commonly called the fork offset distance)
- L_4: the horizontal distance from the center of the rear wheel to the center of mass of the frame/rider
- L_5: the vertical distance from the center of the rear wheel to the center of mass of the frame/rider
- L_6: the distance from the center of the front wheel to the location of the center of mass of the front fork that is perpendicular to the head tube axis
- L_7: the distance from the center of the front wheel to the location of the center of mass of the front fork that is parallel to the head tube axis

Additionally three more reference frames were used to determine the configuration of the four rigid bodies in the Newtonian reference frame, N. These are A the yaw frame, B the roll frame and E the head tube frame. Figure 4 shows how the seven reference frames and eight generalized coordinates define the configuration of the four rigid bodies within the Newtonian frame.
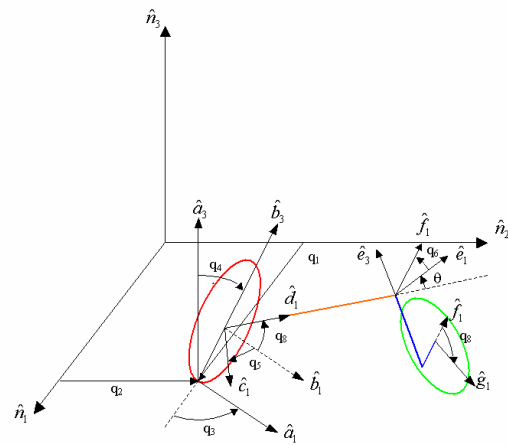

Figure 4: Diagram of the generalized coordinates

The descriptions of the generalized coordinates are as follows:

2

- q_1: location of the contact point of the rear wheel and the ground plane in the n_1 direction
- q_2: location of the contact point of the rear wheel and the ground plane in the n_2 direction
- q_3: describes the simple rotation of reference frame A in N or the yaw (or heading) angle of the rear wheel
- q_4: describes the simple rotation of reference frame B in A or the roll angle of the rear wheel
- q_5: describes the simple rotation of rigid body C in reference frame B or the angular rotation of the rear wheel
- q_6: describes the simple rotation of reference frame F in E or the steering angle
- q_7: describes the simple rotation of rigid body G in reference frame F or the angular rotation of the front wheel
- q_8: describes the simple rotation of the rigid body D in reference frame B or the pitch angle of the frame/rider

Several important points must also be defined.

- N_o: Newtonian origin
- C_o, D_o, F_o, G_o: centers of mass for each rigid body
- N_c: rear wheel contact point on the ground
- C_n: rear wheel contact point on the rear wheel
- N_g: front wheel contact point on the ground
- G_n: front wheel contact point on the front wheel

All eight generalized coordinates are not needed to fully describe the configuration of the system due to the fact that both of the wheels must be in contact with the ground at all times. Mathematically speaking, the vector from the rear wheel contact point, N_c, to the front wheel contact point, N_g, must not have a component in the $\hat{n}_3$ direction, thus the following relationship must hold.

$$\bar{r}^{N_g/N_c} \cdot \hat{n}_3 = 0 \tag{1}$$

To determine the needed position vector, direction cosine matrices for each simple rotation were calculated along with intermediate position vectors. These calculations were determined symbolically in the AUTOLEV program FINDQ8.AL which is included in Appendix 2.

The calculation of the position vector from the center of the front wheel to the front wheel contact point, $\bar{r}^{G_n/G_o}$, wasn't as straightforward as the other position vectors. The direction cosine matrix relating reference frames N and F was known and the fact that $\hat{f}_2$ is always perpendicular to $\bar{r}^{G_n/G_o}$ allowed the vector to be determined to be:

$$\bar{r}^{G_n/G_o} = R_f \frac{\left(\hat{f}_2 \cdot \hat{n}_3\right)\hat{f}_2 - \hat{n}_3}{\left\|\left(\hat{f}_2 \cdot \hat{n}_3\right)\hat{f}_2 - \hat{n}_3\right\|} \tag{2}$$

It turned out that the constraint dot product, (1), was a nonlinear function of the pitch, steer, and roll angles:

$$\bar{r}^{N_g/N_c} \cdot \hat{n}_3 = f\left(q_4, q_6, q_8\right) = 0 \tag{3}$$

This function was linearized about $q_8 = 0$ using a first order Taylor series expansion so that q_8 could be algebraically solved for in terms of the two remaining variables.

$$q_8 = f\left(q_4, q_6\right) \tag{4}$$

This left q_8 as a dependent variable and reduced the number of generalized coordinates required to seven. FINDQ8.AL also computes the first time derivative of q_8 for use in the second program, BICYCLE14.AL.
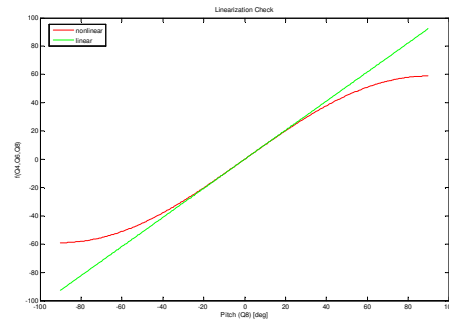

Figure 5: Linearization of $\bar{r}^{N_g/N_c} \cdot \hat{n}_3$ with $q_4 = q_6 = 0$ about $q_8 = 0$

Several checks were made using MATLAB to verify that the equation developed for q_8 was correct. The corresponding MATLAB code,

pitch.m, is included in Appendix 3. Figure 5 shows that the Taylor series expansion successfully linearized the dot product about $q_8=0$.

Figure 6 shows four graphs where either q_4 or q_6 was held constant, while the other independent variable was varied to see if the pitch behaved as anticipated. Each check did as expected thus confirming that the equation for pitch was correct.
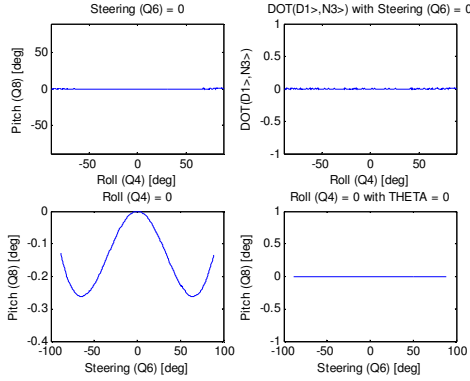

Figure 6: Pitch behavior

Equations of Motion

Now that the configuration coordinates were minimized the equations of motion could be developed. Kane's method was used to derive the equations. Kane's method involves calculating the partial velocities and angular velocities of each rigid body in the system and also the partial velocities and angular velocities of any points that forces and torques may act upon. The partial velocities, forces, torques, accelerations, masses, and inertia quantities can then be formulated into $\widetilde{F}_r + \widetilde{F}_r^*$ where $\widetilde{F}_r$ are the generalized active forces resulting from external forces and torques applied to the system and $\widetilde{F}_r^*$ are the forces resulting from the acceleration of the system. Details of Kane's method can be found in [1].

AUTOLEV, a symbolic manipulation program that easily employs Kane's method for dynamic systems, was used to do the grunt work of the calculations. The following will describe some of the details in developing the AUTOLEV code, BICYCLE14.AL which can be found in Appendix 4.

The same constants and points described in the previous section were used in addition to the following mass and inertia properties. All of the inertia tensors are about the center of mass with

reference to the particular rigid body's local reference frame.

- MC, MD, MF, MG: the mass of each rigid body

- $\begin{bmatrix} IC11 & 0 & 0 \\ 0 & IC22 & 0 \\ 0 & 0 & IC33 \end{bmatrix}$: the inertia tensor

  of the front wheel

- $\begin{bmatrix} ID11 & ID12 & ID31 \\ ID23 & ID22 & ID23 \\ ID31 & ID12 & ID33 \end{bmatrix}$: the inertia tensor

  of the frame/rider

- $\begin{bmatrix} IF11 & IF12 & IF31 \\ IF23 & IF22 & IF23 \\ IF31 & IF12 & IF33 \end{bmatrix}$: the inertia tensor

  of the front fork

- $\begin{bmatrix} IG11 & 0 & 0 \\ 0 & IG22 & 0 \\ 0 & 0 & IG33 \end{bmatrix}$: the inertia tensor

  of the front wheel

The direction cosine matrices describing the rotation of each reference frame were then calculated. The only difference from the direction cosines in FINDQ8.AL was that the function for q8 was inserted which eliminated the dependent generalized coordinate.

Two additional position vectors were created to locate the mass centers of the frame/rider and the front fork.

The kinematical differential equations were chosen in such a manner that the seven generalized speeds simply equaled the derivatives of the seven generalized coordinates.

$$u_r = \dot{q}_r \qquad (5)$$

The velocities of several important points could then be calculated. The velocity of each center of mass was needed along with the velocities of points C_n and G_n which were needed to calculate the non-holonomic constraint equations. The force due to gravity is the only force acting on the system, so no additional velocities were needed.

Due to the previous assumption of no-slip rolling for both of the wheels, four non-holonomic constraint equations could be derived. The velocities of points C_n and G_n in the ground plane must be equal to zero to enforce no-slip rolling so equations (6) and (7) must hold true.

$$^N\overline{v}^{C_n} \cdot \hat{n}_1 = {}^N\overline{v}^{C_n} \cdot \hat{n}_2 = 0 \qquad (6)$$

$$^N\bar{v}^{G_n} \cdot \hat{n}_1 = ^N\bar{v}^{G_n} \cdot \hat{n}_2 = 0 \qquad (7)$$

These dot products create four equations that are linear with respect to the seven generalized speeds, thus they can be algebraically solved to eliminate four of the generalized speeds. The rear wheel angular speed, u_5, the roll rate, u_4, and the steering rate, u_6 were chosen as the independent generalized speeds, which are typical choices in most of the related literature. The remaining dependent generalized speeds: u_1, u_2, u_3, and u_7 were solved for in terms of the independent generalized speeds. This reduced the degrees of freedom of the system from seven to three.

Next the angular accelerations of the four rigid bodies were computed along with the linear accelerations of the mass centers of each body.

The four forces due to the acceleration due to gravity in the $-\hat{n}_3$ direction were then applied to the mass centers of each body.

This provided AUTOLEV with enough information to calculate the equations of motion in the form: $\tilde{F}_r + \tilde{F}_r^* = 0$ where r is number of degrees of freedom of the non-holonomic system. The three equations of motion are linear in terms of the accelerations $\dot{u}_4, \dot{u}_5$, and $\dot{u}_6$. These accelerations were solved for thus putting the equations of motion in the form:

$$\dot{u}_4 = f(u_4, ..., u_6, q_1, ..., q_7) \qquad (8)$$
$$\dot{u}_5 = f(u_4, ..., u_6, q_1, ..., q_7) \qquad (9)$$
$$\dot{u}_6 = f(u_4, ..., u_6, q_1, ..., q_7) \qquad (10)$$

Finally a MATLAB m-file was generated that could simulate the system from initial conditions. This code contained the equations of motion that could also be used for further linearization study.

Simulation

Simulation wasn't necessary to accomplish the goals of this study but one simulation was run to help verify that the equations of motion were correct. Schwab outlines a benchmark bicycle model in his paper [2] that was used for comparison. He presents one nonlinear simulation that was reproduced with the simulation code created in AUTOLEV. Schwab's parameters were converted to the ones described in the *Model Description* section in

schwab.m, which is included in Appendix 5. The initial conditions were matched to Schwab's and were as follows:

$$q_1 = ... = q_7 = 0 \qquad (11)$$
$$(u_4, u_5, u_6) = \left(0.5 rad/s, \frac{4.5 m/s}{R_r}, 0\right) \qquad (12)$$

Figure 7 shows the results of the simulation that can be directly compared to Figure 3 in Scwhab's paper. The plot shows the roll rate, u_4, the steer rate, u_5, and the velocity of the center of the rear wheel, $v = u_5 R_r$. The simulation turned out not to be identical with Schwab's. The velocity has a higher initial peak and it settles to a lower value than in Schwab's simulation. But the general characteristics of the simulation match. This suggests that the equations are basically correct. The causes of the differences in the simulation are not yet understood but further comparison of the linearized model will be detailed in the following section.
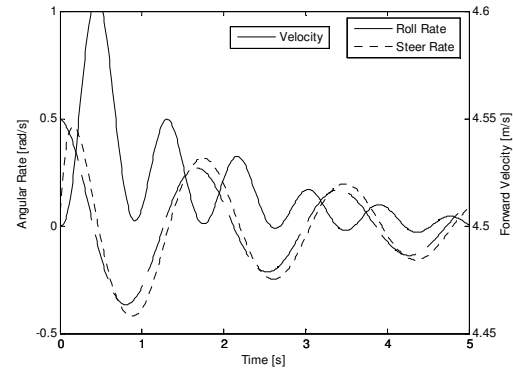
Figure 7: Non-linear simulation

Linearization of Equations of Motion

The previous simulation showed that the roll and steer rates decayed in an exponential oscillatory fashion back to the nominal configuration for that particular velocity. To determine if this is the case for all velocities without running a large amount of simulations the equations can be linearized and the system dynamics matrix can be formed. The eigenvalues of the system dynamics matrix can then be examined to determine whether the system is unstable or not. In general the kinematical differential equations and the equations of motion take the form:

$$\dot{q}_r = f(q_1,...,q_r,u_1,...,u_r) \qquad (13)$$

$$\dot{u}_r = f(q_1,...,q_r,u_1,...,u_r) \qquad (14)$$

These equations can be linearized about a nominal configuration using a multivariable first order Taylor Series expansion. The expansion about the nominal configuration takes the form:

$$f(x_1,...,x_n) =$$
$$f(x_1^{nom},...,x_n^{nom}) + \frac{\partial f(x_1^{nom},...,x_n^{nom})}{\partial x_1}x_1 \qquad (15)$$
$$+...+ \frac{\partial f(x_1^{nom},...,x_n^{nom})}{\partial x_n}x_n$$

The nominal configuration that is of interest is the upright bicycle traveling with a constant rear wheel angular velocity. If u_5 is constant then $\dot{u}_5 = 0$ and the system can be reduced to four equations.

$$\dot{q}_4 = f(q_1,...,q_7,u_4,...,u_6) \qquad (16)$$

$$\dot{q}_6 = f(q_1,...,q_7,u_4,...,u_6) \qquad (17)$$

$$\dot{u}_4 = f(q_1,...,q_7,u_4,...,u_6) \qquad (18)$$

$$\dot{u}_6 = f(q_1,...,q_7,u_4,...,u_6) \qquad (19)$$

These four equations can then be linearized using equation (15) to produce the system dynamics matrix shown in (20).

$$\begin{bmatrix} \dot{q}_4 \\ \dot{q}_6 \\ \dot{u}_4 \\ \dot{u}_6 \end{bmatrix} = \begin{bmatrix} \frac{\partial \dot{q}_4}{\partial q_4} & \frac{\partial \dot{q}_4}{\partial q_6} & \frac{\partial \dot{q}_4}{\partial u_4} & \frac{\partial \dot{q}_4}{\partial u_6} \\ \frac{\partial \dot{q}_6}{\partial q_4} & \frac{\partial \dot{q}_6}{\partial q_6} & \frac{\partial \dot{q}_6}{\partial u_4} & \frac{\partial \dot{q}_6}{\partial u_6} \\ \frac{\partial \dot{u}_4}{\partial q_4} & \frac{\partial \dot{u}_4}{\partial q_6} & \frac{\partial \dot{u}_4}{\partial u_4} & \frac{\partial \dot{u}_4}{\partial u_6} \\ \frac{\partial \dot{u}_6}{\partial q_4} & \frac{\partial \dot{u}_6}{\partial q_6} & \frac{\partial \dot{u}_6}{\partial u_4} & \frac{\partial \dot{u}_6}{\partial u_6} \end{bmatrix}_{nom} \begin{bmatrix} q_4 \\ q_6 \\ u_4 \\ u_6 \end{bmatrix} \qquad (20)$$

Due to memory limits in the educational version of AUTOLEV, the system dynamic matrix could not be calculated symbolically thus preventing the system to be put into the "canonical" form used in [2] and [3]. So the partial derivatives needed to define the matrix were calculated numerically using the definition of the partial derivative shown in (21). These calculations are shown in bike_inertia.m in Appendix 1.

$$\frac{\partial f}{\partial x_m} = \lim_{h \to 0}$$
$$\frac{f(x_1,...,x_m + h,...,x_n) - f(x_1,...,x_m,...,x_n)}{h} \qquad (21)$$

As a check to the validity of the linearized equations of motion that were developed in (20), the numerical values of the system matrix for a particular velocity can be compared to the numerical values given by Schwab's linearized equations. Once again, Schwab's parameters were converted to the ones in the *Model Description* section and the matrix was computed for a rear wheel angular speed of 16.63 rad/s. The calculated values are shown in (22).

$$\begin{bmatrix} 0 & 0 & 1 & 0 \\ 0 & 0 & 0 & 1 \\ 9.465 & -22.733 & -0.523 & -1.631 \\ 12.474 & -18.768 & 18.032 & -15.747 \end{bmatrix} \qquad (22)$$

Schwab's canonical numeric matrices were then transformed into the single system matrix for comparison. Schwab's numerical values are shown in (23).

$$\begin{bmatrix} 0 & 0 & 1 & 0 \\ 0 & 0 & 0 & 1 \\ 9.470 & -22.669 & -0.519 & -1.635 \\ 12.400 & -19.295 & 18.053 & -15.662 \end{bmatrix} \qquad (23)$$

It can be seen that the linearized AUTOLEV equations of motion do not produce the same values as Schwab's. Most are relatively close but one entry has almost a three percent relative difference.

The value of linearizing the equations of motion and building the system dynamics matrix lies in the eigenvalues of the matrix. If any of the eigenvalues have positive real parts then the system is unstable and will not recover from perturbations. The eigenvalues can be determined for a range of speeds encountered when riding a bicycle and plotted. Figure 8

shows a plot of the real parts of the eigenvalues for a rear wheel velocity from 0 to 10 m/s.
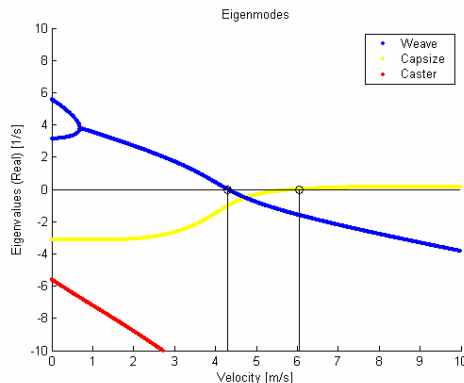

Figure 8: Real parts of the eigenvalues

Three distinct eigenmodes are identifiable. The blue represents the weave mode, the yellow represents the capsize mode and the red represents the caster mode. The weave and the capsize modes both have positive real parts at various speed ranges thus indicating instability.

There are two velocities indicated on Figure 8 that are of interest. One is the velocity at which the weave mode becomes stable, v_w, and the other is the velocity at which the capsize mode becomes unstable, v_c. These two velocities bound a stable speed range in which the bicycle will recover from perturbations.

The weave mode has two distinct real values at very low speeds and the bicycle simply acts like an inverted pendulum. If it is perturbed the bicycle will simply fall over. At a certain speed the weave eigenvalues merge into an imaginary conjugate pair. Above this speed the eigenmode takes on an oscillatory motion when perturbed and will not recover from the perturbation while below the weave critical velocity.

The capsize eigenmode is real at all speeds and the bicycle will fall over in a spiraling fashion if perturbed above the capsize critical velocity. The capsize mode is easily controlled because the eigenvalues are so close to zero as pointed out in [2] thus the capsize critical velocity usually has little practical significance.

One final comparison between Schwab's equations of motion and the ones presented here are an overlay of the eigenvalue plots. Figure 9 shows that the eigenvalues are slightly different and produce different critical velocities. It is unknown at this point why there is a variation in the equations of motion developed here and the ones developed by Schwab. More investigation is needed to find the source of the error.
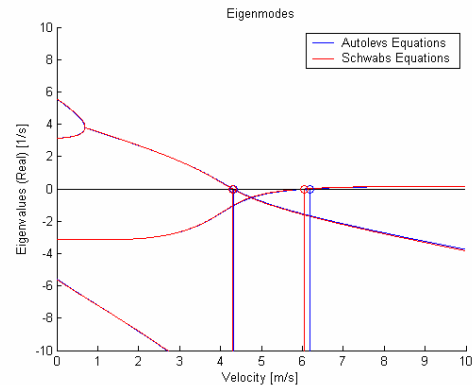

Figure 9: Eigenvalue comparisons

Results

Now that the two critical velocities have been determined for various geometric parameters, plots were developed showing the change in the critical velocities with respect to change in the four geometric parameters that were of interest.

In terms of handling characteristics a lower weave critical velocity would require less control from the rider at a lower speed. This would be very useful for beginning riders, because they would be assisted by the self-stabilization that the bicycle offers without having to ride at a higher speed.

The capsize critical velocity has less significance to handling as mentioned in [2], but if this velocity happens to be higher than the normal operating range of the bicycle then extra control will never be required from the rider to stabilize this mode. Typical road riding speeds are under 13 m/s with higher speeds sometimes reached in downhill descents.

So the only conclusions that can be confidently gleaned from the following plots is whether or not the bicycle will be more or less stable at lower speeds.

Figure 10 shows a plot of front wheel diameter versus the two critical velocities and Figures 11 and 12 show the bicycle geometric configuration for the smallest wheel and the largest wheel checked. When the front wheel diameter is increased the mass and the inertia of the wheel are also increased due to the program design. Figure 10 shows that both of the critical velocities decrease as the wheel size increases. It isn't possible to know whether the diameter, mass, or inertia have the greatest effect. A similar graph in [3] shows only front wheel inertia versus critical velocities and it is shown

that inertia alone decreases the weave critical velocity. But in general as the front wheel size increases the bike self-stabilizes at lower speeds.
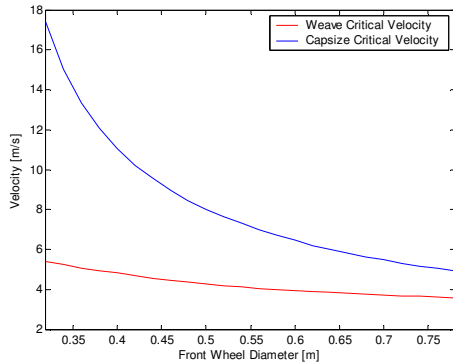

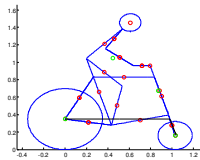Figure 10: Effects of front wheel size
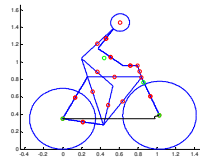

Figure 11: Smallest wheel

Figure 12: Largest wheel

Figure 13 shows the effect of changing the head tube angle on the critical velocities. The following figures, 14 and 15, once again show the two extreme configurations. As the head tube angle becomes steeper the weave critical velocity decreases while the capsize critical velocity increases.
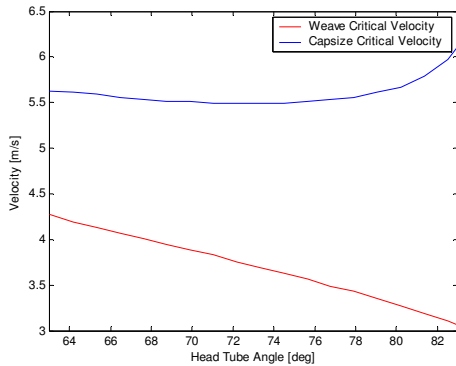
Figure 13: Effects of head tube angle
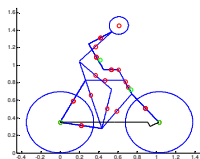
Figure 14: Shallowest head tube angle
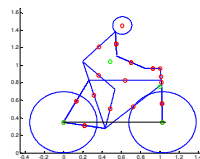
Figure 15: Steepest head tube angle

Figure 16 shows trail versus critical velocities. Trail is the geometrical parameter most often associated with handling. A seasoned bicycle designer, Tim Paterek, states that trail should fall in the range of 0.05 m to 0.065 m for the bike to have comfortable handling. He says that a smaller trail will cause the bicycle to be "twitchy" making the bicycle less manageable and that a larger trail will cause the handling to be more "relaxed".[4] No correlation between the data shown in Figure 16 and Patarek's comfort range can be seen. Although, it is shown that as the trail increases both of the critical velocities increase. The weave critical velocity decreases as the trail decreases, thus making the bike more stable at lower speeds. The capsize critical velocity drops sharply as trail decreases and may influence the controllability of the bicycle more than in previous cases.
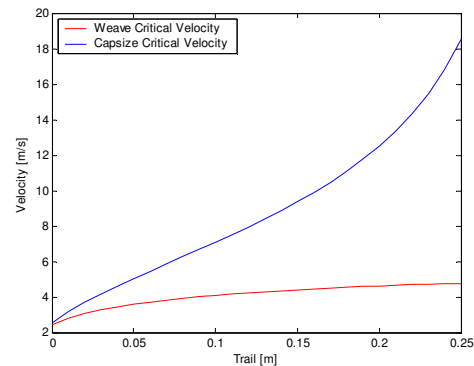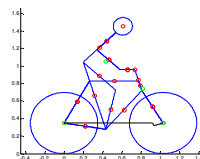

Figure 16: Effects of trail
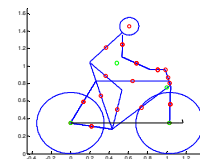

Figure 17: Zero trail

Figure 18: Largest trail

Figure 19 shows how the change in wheelbase affects the critical velocities. Both of the critical velocities increase in a linear fashion with similar slopes as the wheelbase is increased. Longer wheelbase bicycles such as tandems and recumbents seem to usually be more difficult to control at lower speeds so this corresponds with the graph.
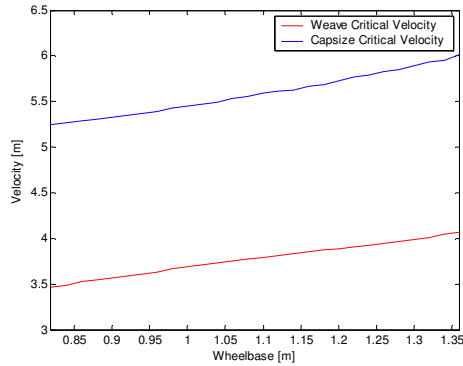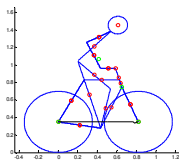
Figure 19: Effects of wheelbase
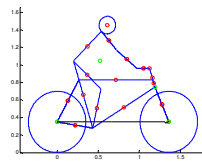

Figure 20: Smallest wheelbase

Figure 21: Largest wheelbase

These four graphs can give some insight into bike design, but mainly only to help create a bicycle that is more stable at lower speeds. It is difficult to extract any criteria that would describe how responsive or sluggish different bicycle configurations are at normal riding speeds. An examination of this model using more in-depth control theory may be able to provide this kind of information. Also correlating this study with a rider's assessment of handling qualities of different frame geometry could provide a valuable set of guidelines for designing bicycles.

References

[1] Kane, T. R., and Levinson, D. A., *Dynamics Online: Theory and Implementation with AUTOLEV*, Online Dynamics, Inc., Sunnyvale, CA, 2000.

[2] Schwab, A. L., Meijaard, J. P., and Papadopoulos, J. M., "Benchmark results on the linearized equations of motion of an uncontrolled bicycle," in *Proc. 2nd Asian Conf. Multibody Dynamics*, Aug. 1-4, 2004, Seoul, Korea, 2004, pp. 143-151.

[3] Astrom, K. J., Klein, R. E., and Lennartsson, A., "Bicycle Dynamics and Control: Adapted bicycles for education and research," IEEE Control Systems Magazine, Aug. 2005, pp. 26-47.

[4] Paterek, T., *The Paterek Manual for Bicycle Framebuilders*, Henry James Bicycles, Inc., Redondo Beach, CA, 2004.